# Immersion and invariance adaptive controller and mixer for coaxial tilt-rotor UAV

Chen, Longlong; Jia, Yanmei; Sun, Sihao; Lv, Zongyang; Wu, Yuhu

**DOI**
10.1016/j.isatra.2025.07.015

**Publication date**
2025

**Document Version**
Final published version

**Published in**
ISA Transactions

ISA Transactions 166 (2025) 353–363

Contents lists available at ScienceDirect

ISA Transactions

journal homepage: www.elsevier.com/locate/isatra

Practice article

# Immersion and invariance adaptive controller and mixer for coaxial tilt-rotor UAV

Longlong Chen[a], Yanmei Jia[b], Sihao Sun[c], Zongyang Lv[d,*], Yuhu Wu[a]

[a] School of Control Science and Engineering and Key Laboratory of Intelligent Control and Optimization for Industrial Equipment of Ministry of Education, Dalian University of Technology, No. 2 Linggong Road, Ganjingzi District, Dalian, Liaoning, 116024, China
[b] School of Science, Dalian Minzu University, No. 18 Liaohe West Road, Economic and Technological Development Zone, Dalian, Liaoning, 116600, China
[c] Department of Cognitive Robotics (CoR), Delft University of Technology, Mekelweg 5, 2628CD, Delft, Orissa, Netherlands
[d] Department of Electrical and Computer Engineering, University of Alberta, 9211-116 st nw, 11th Floor, DICE Buid, Edmonton, AB, T6G1H9, Canada

## HIGHLIGHTS

- An immersion and invariance adaptive controller with RISE-terms and segmented gains which can estimate disturbance torque and force.
- An improved mixer with higher efficiency that considers special properties of coaxial rotors.
- Real flight experimental tests validating the state tracking performance and parameter estimation performance of the control system.

## GRAPHICAL ABSTRACT

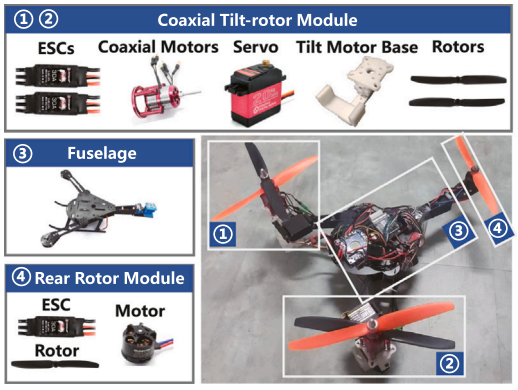


## ARTICLE INFO

*Keywords:*
Adaptive control
Robust control
Coaxial tilt-rotor UAV
Nonlinear control

## ABSTRACT

This study presents a motion control system for a coaxial tilt-rotor (CTR) unmanned aerial vehicle (UAV) equipped with two CTR modules and a tail rotor. The existing adaptive control strategies for CTRUAVs fail to guarantee the theoretical convergence of estimated parameters to their true values. Additionally, the existing mixer requires frequent and inefficient adjustments of the tilt angles for motion control. To address these issues, this work proposes a control strategy that integrates a robust integral of the sign of the error (RISE)-based immersion and invariance (I&I) adaptive controller with segmented gains and an improved mixer. The RISE-based adaptive controller is theoretically capable of estimating and compensating for external disturbance torques and forces with bounded derivatives. Furthermore, a model of the CTR module that accounts for differences between the upper and lower rotors is introduced, and the proposed mixer is designed to realize efficient control at varying tilt angles of the CTR modules. Experimental results demonstrate that the proposed control scheme significantly improves stability, transient response speed, disturbance rejection performance, and parameter estimation accuracy compared to existing control strategies for the CTRUAV.

* Corresponding author.
*Email addresses:* chenlonglongdlut@163.com (L. Chen), jym@dlnu.edu.cn (Y. Jia), sihao.sun@outlook.com (S. Sun), zongyan3@ualberta.ca (Z. Lv), wuyuhu@dlut.edu.cn (Y. Wu).

https://doi.org/10.1016/j.isatra.2025.07.015
Received 16 August 2024; Received in revised form 7 July 2025; Accepted 7 July 2025
Available online 12 July 2025

## 1. Multimedia material

The experimental results are demonstrated in these videos:
https://youtu.be/-puC8TEs5p8,
https://youtu.be/WB87WawTXSQ.

## 2. Introduction

In the last decade, unmanned aerial vehicles (UAVs) have seen significant advancements in their capabilities. As a result, UAVs have been widely employed in various complex and hazardous tasks, including transportation, atmospheric monitoring, fire protection, rescue operations, circuit inspection, and aerial photography [12,21,28]. UAVs primarily fall into the following categories: fixed-wing UAVs, multi-rotor UAVs, helicopter UAVs, and tilt-rotor UAVs (TRUAVs). Despite the increased complexity in mechanical structure and control design, TRUAVs offer the combined advantages of vertical flight capability, high maneuverability and cruising speed [9,15,23,35].

Considering the aforementioned challenges and inherent structural advantages, the control design for Tilt-Rotor Unmanned Aerial Vehicles (TRUAVs) has become a prominent research area. Recent studies have investigated various TRUAV configurations. A significant portion of the research focuses on tilt dual-rotor UAVs, including the Bell Eagle Eye [27], the Smart Unmanned Aerial Vehicle developed by the Korea Aerospace Research Institute [38], and dual tilt-wing UAVs such as HARVee [17]. These tilt dual-rotor UAVs feature complex mechanical structures enabling cyclic control of the propellers, which is crucial for stabilization and maneuverability. The tilt tri-rotor UAV configuration provides an efficient alternative by avoiding the complexity of variable-pitch structures. For instance, Papachristos et al. introduced a tilt tri-rotor UAV, developed a nonlinear dynamic model, and designed a nonlinear control system tailored to its characteristics [25]. Amato et al. developed a nonlinear dynamic inversion-based controller for tilt tri-rotor UAVs, enhancing robustness against parametric variations [9]. Chen et al. designed a tilt tri-rotor UAV and implemented a cascaded conversion control system, achieving stable flight and rapid transition [6]. Xian and Hao proposed a continuous nonlinear robust fault-tolerant controller for a tilt tri-rotor UAV powered by three motors and a tail servo [35]. Additionally, a coaxial tilt-rotor UAV (CTRUAV) featuring two pairs of CTR modules and a tail rotor, as shown in Fig. 1, was introduced in [24]. The CTRUAV only requires adjusting the tilt angles of the CTR modules, rather than tilting the entire fuselage as in quadrotor UAVs, to perform agile forward or backward flight maneuvers. Furthermore, the CTRUAV can reduce flight resistance by actively adjusting its angle of attack. Furthermore, while it is well known that efficiency is higher with fewer large-diameter rotors, coaxial rotors offer distinct advantages over single rotors: a more compact structure, higher thrust, and reduced Coriolis forces on the rotors, which significantly decrease the load on the tilt servos [8,18,22,32]. Consequently, the coaxial-rotor scheme has been successfully applied in various aircraft, such as the S-97 RAIDER helicopter [3] and the Ingenuity Mars helicopter [34].

Despite the aforementioned advantages of the CTRUAV, controlling such an underactuated nonlinear system is a challenging work due to the inevitable presence of various disturbances caused by external interference, payload, and the coupled turbulence caused by coaxial rotors. Adaptive control is an effective method that compensates for the uncertainties and external disturbances of different mechanical systems, as detailed in [11,20,33,37]. In [24], we employed a conventional adaptive control strategy for the CTRUAV's attitude tracking. However, this adaptive control method is based on the certainty equivalence (CE) principle, by which the parameter estimation and controller design are conducted simultaneously. As a result, the adaptive update law in [24] relates solely to the system state error and is independent of the estimates of the uncertain terms. Consequently, the estimated parameter cannot theoretically converge to its true value [30].

In [7,29], I&I-based adaptive attitude controllers are developed specifically to control the attitude and estimate the rotational damping coefficients. Furthermore, due to the mixer's constraint requiring the coaxial rotors to maintain identical rotational rates [19,24], the CTR modules must generate component forces pointing in opposite directions along the axis $X_b$ to produce a torque around the axis $Z_b$. This results in inefficient internal force cancellation and energy inefficiency. Moreover, employing the mixer in [19,24] necessitates frequent adjustments of the tilt angles to maintain the CTRUAV's attitude. This significantly increases the risk of servo-stuck faults, making it unsuitable for scenarios involving CTR modules with high rotational inertia. It should be noted that these issues related to the mixer are inevitable for classic tilt tri-rotor UAVs due to single-rotor configuration [6,10,31,39,40].

Considering the aforementioned issues, this work proposes an improved control strategy for the CTRUAV. The newly developed strategy integrates an Immersion and Invariance (I&I) adaptive controller with robust integral of the Sign of the Error (RISE)-based terms, segmented gains, and an improved mixer designed for higher efficiency. The key contributions are detailed as follows:

1) RISE-based I&I adaptive controller: The I&I theory, a Non-Certainty-Equivalence (Non-CE) theory pioneered by Astolfi et al. [2,16], has been studied by researchers and combined with adaptive control laws in [1,39]. The RISE-based control structure is used to compensate for uncertain disturbances [13,26,36]. The proposed RISE-based I&I adaptive controller offers several advantages over classic I&I adaptive controllers [7,29] and conventional adaptive controllers [24]. By introducing RISE-based adaptive correction terms for the unknown time-varying disturbance torques and forces, disturbance adaptive estimation and controller design are conducted separately, effectively eliminating the direct coupling between adaptive estimation errors and state errors. As a result, the estimation of time-varying disturbance torques and forces can theoretically converge to their true values [1,14]. Furthermore, the segmented gains in the PD-like terms and the I&I-based adaptive laws in the proposed controller can further enhance the transient response speed and disturbance-rejection capability of the CTRUAV compared to the existing methods in [7,29].
2) Mixer: Considering the rotor downwash of the upper rotor on the lower rotor, measurement tests are conducted to reveal this asymmetric property. Performance models of the CTR module, which account for the differences between the upper and lower rotors, are constructed. Based on this model and the CTRUAV's specific configuration, a nonlinear mixer is developed. This mixer ensures that attitude control is achieved solely by adjusting the rotational rates of the rotors while keeping the CTR modules at fixed tilt angles. The tilt angles of the CTR modules are used exclusively for adjusting the CTRUAV's forward thrust. As a result, the inefficient internal force cancellation problem is resolved, and the load on the servos is significantly reduced.
3) Experiments: Experiments are conducted under different scenarios: (i) stabilization for attitude tracking under external torques; (ii) velocity control in the presence of unknown disturbance forces. The results of these tests demonstrate a significant improvement in the performance of the proposed control scheme compared to existing methods for the CTRUAV.

The structure of this paper is outlined as follows: Section 3 presents the mathematical model for the dynamics of the CTRUAV. In Section 4, we develop the improved mixer and the I&I-based adaptive controller. The performance and effectiveness of the proposed control system are demonstrated and validated through experiments in Section 5. Finally, Section 6 concludes the paper with a summary of the findings and contributions.

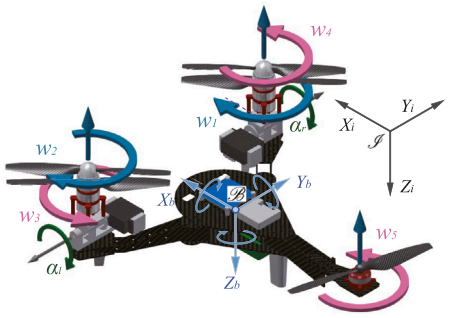


**Fig. 1.** Structure of the CTRUAV.

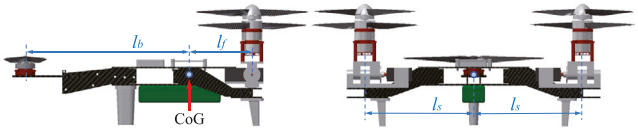


**Fig. 2.** Key dimensions of the CTRUAV prototype.

## 3. Dynamic model

The rotational inertia of the CTR module is $0.33 \times \mathrm{g} \cdot \mathrm{m}^2$ around the rotation axis of the tilt servos, which is less than 3.65 % of the total rotational inertia $8.99 \times \mathrm{g} \cdot \mathrm{m}^2$ of the CTRUAV. For simplification, the CTRUAV is modeled as a single rigid body, and the pitch torque caused by the tilt motion of the CTR modules is simplified as a torque acting on the body of the CTRUAV. We define two reference frames to describe the attitude and position of the CTRUAV, as shown in Fig. 1: the inertial frame $\mathscr{I}\{X_i, Y_i, Z_i\}$ and the CTRUAV's body frame $\mathscr{B}\{X_b, Y_b, Z_b\}$. The origin of $\mathscr{B}\{X_b, Y_b, Z_b\}$ coincides with the CTRUAV's center of gravity (CoG). In these reference frames, the coordinates are defined: $\boldsymbol{\xi} = [x\ y\ z]^\top \in \mathbb{R}^3$ represents the CoG of the CTRUAV in inertial frame $\mathscr{I}$; $\boldsymbol{\eta} = [\phi\ \theta\ \psi]^\top \in \mathbb{R}^3$ represents the CTRUAV's Euler angles. Currently, we do not consider the case of performing aggressive maneuvers, and the attitude angle $\boldsymbol{\eta}$ is constrained by

$$\phi, \theta \in (-\pi/2, \pi/2). \tag{1}$$

The key dimensions of the CTRUAV are illustrated in Fig. 2. $l_b$ represents the distance from the tail rotor's rotational axis to the CoG of the CTRUAV along direction $X_b$, while $l_f$ and $l_s$ denote the distances from the CTR modules to the CTRUAV's CoG along directions $X_b$ and $Y_b$, respectively. In this study, the symbols $\boldsymbol{s}$ and $\boldsymbol{c}$ represent the sine and cosine functions, respectively; $\mathbf{0}_{m\times n}$ denotes the null matrix of dimensions $m \times n$; $\boldsymbol{I}_n$ represents the identity matrix of dimension $n$; For vectors $\boldsymbol{x} = [x_1\ x_2\ \dots\ x_n]^\top$ and $\boldsymbol{y} = [y_1\ y_2\ \dots\ y_n]^\top$, we define $\mathrm{sgn}(\boldsymbol{x}) = [\mathrm{sign}(x_1)\ \mathrm{sign}(x_2)\ \dots\ \mathrm{sign}(x_n)]^\top$, and the Hadamard product as $\boldsymbol{x} \circ \boldsymbol{y} = [x_1 y_1\ x_2 y_2\ \dots\ x_n y_n]^\top$.

The dynamic model of the CTRUAV was initially introduced in [24]. For the sake of clarity and completeness, an overview of the model is presented in this section:

$$\ddot{\boldsymbol{\xi}} = m^{-1}\left(\boldsymbol{F}_{\xi} + m\boldsymbol{g} + \boldsymbol{R}_b^i \boldsymbol{D}_{\boldsymbol{\xi b}} + \boldsymbol{F}_s\right), \tag{2a}$$

$$\ddot{\boldsymbol{\eta}} = \boldsymbol{J}_u^{-1}\left(\boldsymbol{\tau}_{\boldsymbol{\eta}} - \dot{\boldsymbol{J}}_u\dot{\boldsymbol{\eta}} + \boldsymbol{C} + \boldsymbol{\tau}_\Gamma + \boldsymbol{D}_{\boldsymbol{\eta}} + \boldsymbol{\tau}_s\right), \tag{2b}$$

where $m$ is the mass of the CTRUAV, $\boldsymbol{J}_u = \boldsymbol{R}_{ev}^{bv\top} \boldsymbol{I}_u \boldsymbol{R}_{ev}^{bv}$, with the rotational inertia matrix $\boldsymbol{I}_u = \mathrm{diag}(I_{xx}, I_{yy}, I_{zz})$ of the CTRUAV in the body frame $\mathscr{B}$, $\boldsymbol{R}_b^i$ denotes the rotation matrix from frame $\mathscr{B}$ to frame $\mathscr{I}$, and $\boldsymbol{R}_{ev}^{bv}$ represents the transformation matrix that converts Euler angular velocity into the angular velocity in frame $\mathscr{B}$ [4]: $\boldsymbol{R}_{ev}^{bv} = \begin{bmatrix} 1 & 0 & -\boldsymbol{s}\theta \\ 0 & \boldsymbol{c}\phi & \boldsymbol{s}\phi\boldsymbol{c}\theta \\ 0 & -\boldsymbol{s}\phi & \boldsymbol{c}\phi\boldsymbol{c}\theta \end{bmatrix}$.

The drag force $\boldsymbol{D}_{\boldsymbol{\xi b}}$ in (2a) and drag torque $\boldsymbol{D}_{\boldsymbol{\eta}}$ in (2b) are given by

$$\boldsymbol{D}_{\boldsymbol{\xi b}}(\dot{\boldsymbol{\xi}}_{\boldsymbol{b}}) = -[D_{xb}\dot{x}_b|\dot{x}_b|\ D_{yb}\dot{y}_b|\dot{y}_b|\ D_{zb}\dot{z}_b|\dot{z}_b|]^\top,$$
$$\boldsymbol{D}_{\boldsymbol{\eta}}(\dot{\boldsymbol{\eta}}) = -[D_\phi\dot{\phi}|\dot{\phi}|\ D_\theta\dot{\theta}|\dot{\theta}|\ D_\psi\dot{\psi}|\dot{\psi}|]^\top,$$

where the coefficients $D_{xb}$, $D_{yb}$, $D_{zb}$, $D_\phi$, $D_\theta$, and $D_\psi$ are measured and obtained through experimental tests in [24], $\dot{\boldsymbol{\xi}}_b = [\dot{x}_b\ \dot{y}_b\ \dot{z}_b]^\top = \boldsymbol{R}_i^b\dot{\boldsymbol{\xi}}$ represents the velocity in frame $\mathscr{B}$.

In (2a), $\boldsymbol{g} = [0\ 0\ g]^\top$ with the gravitational acceleration $g$. In (2b), $\boldsymbol{C} = [C_\phi\ C_\theta\ 0]^\top = \partial(\frac{1}{2}\dot{\boldsymbol{\eta}}^\top \boldsymbol{J}_u\dot{\boldsymbol{\eta}})/\partial\boldsymbol{\eta}$, and $\boldsymbol{\tau}_\Gamma = [0, \tau_{\gamma r} + \tau_{\gamma l}, 0]^\top$ denotes the rotational torque generated by the servos, where $\tau_{\gamma r}$ and $\tau_{\gamma l}$ represent the rotational torques produced by the right and left servos, respectively.

The expression $\boldsymbol{F}_{\boldsymbol{\xi}} = [F_x\ F_y\ F_z]^\top$ denotes the control force generated by the rotor thrust. Meanwhile, $\boldsymbol{\tau}_{\boldsymbol{\eta}} = [\tau_\phi\ \tau_\theta\ \tau_\psi]^\top$ represents the control torque arising from both the thrust and the reaction torque of the rotors. The terms $\boldsymbol{\tau}_{\boldsymbol{s}} = [\tau_{s\phi}\ \tau_{s\theta}\ \tau_{s\psi}]^\top$ in (2b) and $\boldsymbol{F}_{\boldsymbol{s}} = [F_{sx}\ F_{sy}\ F_{sz}]^\top$ in (2a) are external disturbances.

**Assumption 1.** For the CTRUAV, several types of disturbances may be encountered, including aerodynamic torques, aerodynamic forces, and other environmental disturbances caused by rotor downwash. The lumped disturbances are denoted as $\boldsymbol{\tau}_{\boldsymbol{s}}$ and $\boldsymbol{F}_{\boldsymbol{s}}$ in model (2), which are supposed to be time-varying and differentiable with bounded derivatives. Therefore, it is reasonable to simplify and assume that there always exist positive boundaries $\bar{\boldsymbol{\tau}}_{\boldsymbol{ds}} = [\bar{\tau}_{ds\phi}\ \bar{\tau}_{ds\theta}\ \bar{\tau}_{ds\psi}]^\top$ and $\bar{\boldsymbol{F}}_{\boldsymbol{ds}} = [\bar{F}_{dsx}\ \bar{F}_{dsy}\ \bar{F}_{dsz}]^\top$ such that $|\dot{\tau}_{si}| \le \bar{\tau}_{dsi},\ i \in \{\phi, \theta, \psi\}$ and $|\dot{F}_{si}| \le \bar{F}_{dsi},\ i \in \{x, y, z\}$.

## 4. Control strategy

The objective of this work is to develop an I&I-based adaptive control strategy for the CTRUAV to realize attitude and velocity tracking control, enhance transient performance, and estimate external disturbances as described by $\boldsymbol{\tau}_{\boldsymbol{s}}$ in (2b) and $\boldsymbol{F}_{\boldsymbol{s}}$ in (2a). Additionally, we design a different mixer to generate the control inputs $\boldsymbol{F}_{\boldsymbol{\xi}}$ in (2a) and $\boldsymbol{\tau}_{\boldsymbol{\eta}}$ in (2b) to mitigate the inefficiency arising from internal force cancellation problem of the mixer in [19,24]. The architecture of the comprehensive control system is illustrated in Fig. 3.

Before proposing the controller for the CTRUAV, a function is defined as $\boldsymbol{K}(\boldsymbol{x}) = [\mathscr{K}(x_1)\ \mathscr{K}(x_2)\ \mathscr{K}(x_3)]^\top$, for a vector $\boldsymbol{x} = [x_1\ x_2\ x_3]^\top$, where $\mathscr{K}(x)$ is an odd segmented gain function satisfying $\frac{\partial\mathscr{K}(x)}{\partial x} \ge 1$, $\frac{\partial\mathscr{K}(x)}{\partial x} \le \frac{\partial\mathscr{K}(y)}{\partial y}$, with $|x| \ge |y|,\ x,\ y \in \mathbb{R}$.

### 4.1. Mixer design

Despite the CTRUAV's underactuated property, it exhibits overactuation in specific degrees of freedom (DoFs). This phenomenon arises because the seven control inputs, comprising the thrust $F_i$ generated by rotor $i$ and the tilt angles $\alpha_r$ and $\alpha_l$, can directly manipulate five DoFs of the CTRUAV: translations along axes $X_b$ and $Z_b$, and rotations around the three axes. The rotors and servos can not generate thrust force along axis $Y_b$. For every given $\boldsymbol{F}_{\boldsymbol{xzb}}$ and $\boldsymbol{\tau}_{\boldsymbol{\eta}}$, the control signals to the rotors and servos can be obtained by the mixer, as shown in the yellow section of Fig. 3. We define $\boldsymbol{F}_{\boldsymbol{xzb}} = [F_{xb}\ F_{zb}]^\top$, where $F_{xb}$ and $F_{zb}$ represent the component forces produced by the rotors along directions $X_b$ and $Z_b$, respectively. Then, the relationship between $\boldsymbol{F}_{\boldsymbol{\xi}}$ and $\boldsymbol{F}_{\boldsymbol{xzb}}$ is presented as

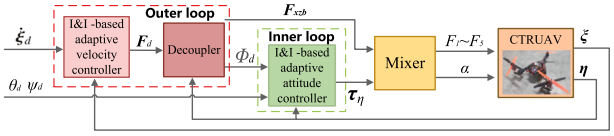


**Fig. 3.** Schematic of the closed-loop control system.

$$\boldsymbol{F}_{\xi} = [F_x \ F_y \ F_z]^{\top} = \boldsymbol{R}\boldsymbol{F}_{\boldsymbol{xzb}}, \tag{3}$$

where $\boldsymbol{R} = \boldsymbol{R}_b^i \begin{bmatrix} 1 & 0 & 0 \\ 0 & 0 & 1 \end{bmatrix}^{\top}$ is the projection matrix. The control torque $\boldsymbol{\tau}_{\boldsymbol{\eta}} = [\tau_\phi \ \tau_\theta \ \tau_\psi]^{\top}$ is composed of $\boldsymbol{\tau}_{\boldsymbol{\eta t}}$ originating from the thrust forces and $\boldsymbol{\tau}_{\boldsymbol{\eta r}}$ produced by the rotors' reaction torques. The term $\boldsymbol{\tau}_{\boldsymbol{\eta t}}$ is calculated by

$$\boldsymbol{\tau}_{\boldsymbol{\eta t}} = \sum_{i=r,l,b} \boldsymbol{r}_i \times \boldsymbol{f}_i,$$

where $\boldsymbol{r}_{\boldsymbol{r}} = [l_f \ l_s \ 0]$, $\boldsymbol{r}_{\boldsymbol{l}} = [l_f \ -l_s \ 0]$, $\boldsymbol{r}_{\boldsymbol{b}} = [-l_b \ 0 \ 0]$, $\boldsymbol{f}_{\boldsymbol{r}} = [-F_r s\alpha_r \ 0 \ -F_r c\alpha_r]$, $\boldsymbol{f}_{\boldsymbol{l}} = [-F_l s\alpha_l \ 0 \ -F_l c\alpha_l]$, $\boldsymbol{f}_{\boldsymbol{b}} = [0 \ 0 \ -F_5]$, with forces $F_r = F_1 + F_4$, $F_l = F_2 + F_3$, and $F_5$ generated by the right CTR module, left CTR module, and the tail rotor, respectively, with the thrust $F_i$ generated by rotor $i$. The torque produced by the reaction torques of the rotors is given by $\boldsymbol{\tau}_{\boldsymbol{\eta r}} = \left[\tau_r s\alpha_r + \tau_l s\alpha_l \ 0 \ \tau_r c\alpha_r + \tau_l c\alpha_l\right]^{\top}$. Then, the relationship between the force $\boldsymbol{F}_{\boldsymbol{xzb}}$, the torque $\boldsymbol{\tau}_{\boldsymbol{\eta}}$, and the thrusts $F_i$ and reaction torques of the rotors is given by

$$\begin{bmatrix} F_{xb} \\ F_{zb} \\ \tau_\phi \\ \tau_\theta \\ \tau_\psi \end{bmatrix} = \begin{bmatrix} -F_r s\alpha_r - F_l s\alpha_l \\ -F_r c\alpha_r - F_l c\alpha_l - F_5 \\ -F_r c\alpha_r l_s + F_l c\alpha_l l_s + \tau_r s\alpha_r + \tau_l s\alpha_l \\ F_r c\alpha_r l_f + F_l c\alpha_l l_f - F_5 l_b \\ F_r s\alpha_r l_s - F_l s\alpha_l l_s + \tau_b + \tau_r c\alpha_r + \tau_l c\alpha_l \end{bmatrix}, \tag{4}$$

where $\tau_r = c_{fu}F_4 - c_{fd}F_1$, $\tau_l = c_{fd}F_3 - c_{fu}F_2$, and $\tau_b = c_b F_5$ are the reaction torques generated by the rear rotor, right and left CTR modules, respectively. The terms $c_b$, $c_{fu}$, and $c_{fd}$ are the coefficients from the thrusts of the tail rotor, the upper rotor and lower rotor of the CTR modules to their corresponding reaction torques, respectively.

To solve (4) and transform $F_{xb}$, $F_{zb}$, $\tau_\phi$, $\tau_\theta$, and $\tau_\psi$ into $F_i$ $(i = 1 \sim 5)$, $\alpha_r$, and $\alpha_l$, we design two constraints as $\alpha = \alpha_r = \alpha_l$, $\tau_r = \tau_l$. Then, the mixer can be obtained as

$$\begin{aligned}
F_5 &= -(F_{zb}l_f + \tau_\theta)/(l_f + l_b), \\
\alpha &= \arctan\left(F_{xb}/(F_{zb} + F_5)\right), \\
F_1 &= (Al_s(c_{fd} + c_{fu}) + 2\,Bc_{fu}s\alpha - 2c_{fu}\tau_\phi c\alpha - 2\,Bl_s c\alpha \\
&\quad - 2l_s\tau_\phi s\alpha)/(4l_s(c_{fd} + c_{fu})), \\
F_2 &= (Al_s(c_{fd} + c_{fu}) - 2\,Bc_{fd}s\alpha + 2c_{fd}\tau_\phi c\alpha - 2\,Bl_s c\alpha \\
&\quad - 2l_s\tau_\phi s\alpha)/(4l_s(c_{fd} + c_{fu})), \\
F_3 &= (Al_s(c_{fd} + c_{fu}) - 2\,Bc_{fu}s\alpha + 2c_{fu}\tau_\phi c\alpha + 2\,Bl_s c\alpha \\
&\quad + 2l_s\tau_\phi s\alpha)/(4l_s(c_{fd} + c_{fu})), \\
F_4 &= (Al_s(c_{fd} + c_{fu}) + 2\,Bc_{fd}s\alpha - 2c_{fd}\tau_\phi c\alpha + 2\,Bl_s c\alpha \\
&\quad + 2l_s\tau_\phi s\alpha)/(4l_s(c_{fd} + c_{fu})),
\end{aligned}$$

where $A = (\tau_\theta + F_5 l_b)/(l_f c\alpha)$, $B = \tau_\psi - c_b F_5$.

**Remark 1.** There are differences in the reaction torque and thrust performance between the upper and lower rotors of the CTR modules, and these factors are taken into account in the mixer. Hence, we define two coefficients $c_{fu}$ and $c_{fd}$ respectively for the upper rotor and lower rotor.

**Remark 2.** The proposed mixer operates under the assumption that $\alpha = \alpha_r = \alpha_l$. By adjusting the thrusts $F_i$ $(i = 1 \sim 5)$, it can generate the component force $F_{zb}$ and torque $\boldsymbol{\tau}_{\boldsymbol{\eta}}$ with any given tilt angle $\alpha$, implying that the tilt angle $\alpha$ is solely utilized for adjusting the component force $F_{xb}$. Unlike the mixer in [19,24], the CTRUAV does not require frequent adjustments of its tilt angles to maintain its attitude. This is particularly beneficial for controlling large-scale CTRUAVs, because the designed mixer can significantly reduces the risk of servo-stuck faults and extends the lifespan of the servos. Moreover, the issue of inefficient internal force cancellation has been addressed. For example, when controlled by the mixer in [19,24], the coaxial rotors are required to produce 6.1 % (sec20° − 1) additional thrust compared to the component force in the $Z_b$-direction at tilt angles of up to 20°. This inefficiency is eliminated by the newly designed mixer. This is a significant superiority compared to the CTRUAV system in [19,24] and classic tilt tri-rotor UAVs [6,10,31,40].

### 4.2. Inner-loop controller

The inner-loop controller is utilized to track the desired attitude $\boldsymbol{\eta}_{\boldsymbol{d}}$. The associated tracking errors $\boldsymbol{e}_{\boldsymbol{\eta}} = [e_\phi, e_\theta, e_\psi]^{\top}$ and $\boldsymbol{e}_{\boldsymbol{d\eta}} = [e_{d\phi}, e_{d\theta}, e_{d\psi}]^{\top}$ are defined as follows:

$$\boldsymbol{e}_{\boldsymbol{\eta}} = \boldsymbol{\eta}_d - \boldsymbol{\eta}, \ \boldsymbol{e}_{\boldsymbol{d\eta}} = \dot{\boldsymbol{e}}_{\boldsymbol{\eta}} + \boldsymbol{\alpha}_{\boldsymbol{\eta}}\boldsymbol{e}_{\boldsymbol{\eta}} \tag{6}$$

where $\boldsymbol{\alpha}_{\boldsymbol{\eta}} = \mathrm{diag}(\alpha_\phi, \alpha_\theta, \alpha_\psi)$ represents a positive definite diagonal matrix. Substituting (2b) into the time derivative of (6) yields

$$\dot{\boldsymbol{e}}_{\boldsymbol{\eta}} = \boldsymbol{e}_{\boldsymbol{d\eta}} - \boldsymbol{\alpha}_{\boldsymbol{\eta}}\boldsymbol{e}_{\boldsymbol{\eta}}, \tag{7a}$$

$$\dot{\boldsymbol{e}}_{\boldsymbol{d\eta}} = -\boldsymbol{J}_u^{-1}\left(\boldsymbol{\tau}_{\boldsymbol{\eta}} + \boldsymbol{\tau}_s\right) + \boldsymbol{\gamma}_{\boldsymbol{\eta}}, \tag{7b}$$

with $\boldsymbol{\gamma}_{\boldsymbol{\eta}} = \ddot{\boldsymbol{\eta}}_d + \boldsymbol{J}_u^{-1}\left(\dot{\boldsymbol{J}}_u\dot{\boldsymbol{\eta}} - \boldsymbol{C} - \boldsymbol{\tau}_\Gamma - \boldsymbol{D}_{\boldsymbol{\eta}}\right) + \boldsymbol{\alpha}_{\boldsymbol{\eta}}\dot{\boldsymbol{e}}_{\boldsymbol{\eta}}$.

Define the estimation error $\boldsymbol{\zeta}_{\boldsymbol{\eta}} = [\zeta_\phi \ \zeta_\theta \ \zeta_\psi]^{\top}$ as

$$\boldsymbol{\zeta}_{\boldsymbol{\eta}} = \hat{\boldsymbol{\tau}}_s + \boldsymbol{\beta}_{\boldsymbol{\eta}}\left(\boldsymbol{e}_{\boldsymbol{\eta}}, \boldsymbol{e}_{\boldsymbol{d\eta}}\right) - \boldsymbol{\tau}_s, \tag{8}$$

where $\boldsymbol{\beta}_{\boldsymbol{\eta}} = [\beta_\phi \ \beta_\theta \ \beta_\psi]^{\top}$ is an auxiliary function that ensures the invariance of the closed-loop system and will be designed later. Differentiating (8) with respect to time yields

$$\dot{\boldsymbol{\zeta}}_{\boldsymbol{\eta}} = \dot{\hat{\boldsymbol{\tau}}}_s + \frac{\partial \boldsymbol{\beta}_{\boldsymbol{\eta}}}{\partial \boldsymbol{e}_{\boldsymbol{\eta}}}\dot{\boldsymbol{e}}_{\boldsymbol{\eta}} + \frac{\partial \boldsymbol{\beta}_{\boldsymbol{\eta}}}{\partial \boldsymbol{e}_{\boldsymbol{d\eta}}}\dot{\boldsymbol{e}}_{\boldsymbol{d\eta}} - \dot{\boldsymbol{\tau}}_s. \tag{9}$$

The control torque $\boldsymbol{\tau}_{\boldsymbol{\eta}}$ is formulated as

$$\boldsymbol{\tau}_{\boldsymbol{\eta}} = \boldsymbol{J}_{\boldsymbol{u}}\boldsymbol{k}_{\boldsymbol{\eta}}\boldsymbol{K}(\boldsymbol{e}_{\boldsymbol{d\eta}}) - (\hat{\boldsymbol{\tau}}_s + \boldsymbol{\beta}_{\boldsymbol{\eta}}) + \boldsymbol{J}_u\boldsymbol{\gamma}_{\boldsymbol{\eta}}, \tag{10}$$

with the RISE-based adaptive update law

$$\dot{\hat{\boldsymbol{\tau}}}_s = \frac{\partial \boldsymbol{\beta}_{\boldsymbol{\eta}}}{\partial \boldsymbol{e}_{\boldsymbol{d\eta}}}\left(\boldsymbol{J}_{\boldsymbol{u}}{}^{-1}(\boldsymbol{\tau}_{\boldsymbol{\eta}} + \hat{\boldsymbol{\tau}}_s + \boldsymbol{\beta}_{\boldsymbol{\eta}}) - \boldsymbol{\gamma}_{\boldsymbol{\eta}}\right) - \frac{\partial \boldsymbol{\beta}_{\boldsymbol{\eta}}}{\partial \boldsymbol{e}_{\boldsymbol{\eta}}}\dot{\boldsymbol{e}}_{\boldsymbol{\eta}} - \mathrm{sgn}(\boldsymbol{\zeta}_{\boldsymbol{\eta}}) \circ \bar{\boldsymbol{\tau}}_{\boldsymbol{ds}}, \tag{11a}$$

$$\boldsymbol{\beta}_{\boldsymbol{\eta}} = -\boldsymbol{\rho}_{\boldsymbol{\eta}}\boldsymbol{J}_{\boldsymbol{u}}{}^{-1}\boldsymbol{K}(\boldsymbol{e}_{\boldsymbol{d\eta}}), \tag{11b}$$

where $\boldsymbol{k}_{\boldsymbol{\eta}} = \mathrm{diag}(k_\phi, k_\theta, k_\psi)$ and $\boldsymbol{\rho}_{\boldsymbol{\eta}} = \mathrm{diag}(\rho_\phi, \rho_\theta, \rho_\psi)$ denote diagonal positive-definite matrices. According to the attitude model (2b), we define

$$\boldsymbol{\tau}_{\boldsymbol{sr}} = \boldsymbol{J}_u\ddot{\boldsymbol{\eta}} - \boldsymbol{\tau}_{\boldsymbol{\eta}} + \dot{\boldsymbol{J}}_u\dot{\boldsymbol{\eta}} - \boldsymbol{C} - \boldsymbol{\tau}_\Gamma - \boldsymbol{D}_{\boldsymbol{\eta}},$$

which is treated as the real disturbance $\boldsymbol{\tau}_s$. Then, the term $\boldsymbol{\zeta}_{\boldsymbol{\eta}}$ in (11a) is obtained $\boldsymbol{\zeta}_{\boldsymbol{\eta}} = \hat{\boldsymbol{\tau}}_s + \boldsymbol{\beta}_{\boldsymbol{\eta}} - \boldsymbol{\tau}_{\boldsymbol{sr}}$. By utilizing the auxiliary function $\boldsymbol{\beta}_{\boldsymbol{\eta}}$, the actual disturbance can be estimated theoretically and subsequently compensated in the closed-loop system. Substituting (7b), (8) and (11) into (9) yields

$$\dot{\boldsymbol{\zeta}}_{\boldsymbol{\eta}} = -\boldsymbol{\rho}_{\boldsymbol{\eta}}\boldsymbol{J}_{\boldsymbol{u}}{}^{-1}\frac{\partial \boldsymbol{K}(\boldsymbol{e}_{\boldsymbol{d\eta}})}{\partial \boldsymbol{e}_{\boldsymbol{d\eta}}}\boldsymbol{J}_{\boldsymbol{u}}{}^{-1}\boldsymbol{\zeta}_{\boldsymbol{\eta}} - \mathrm{sgn}(\boldsymbol{\zeta}_{\boldsymbol{\eta}}) \circ \bar{\boldsymbol{\tau}}_{\boldsymbol{ds}} - \dot{\boldsymbol{\tau}}_s. \tag{12}$$

Substituting (8) and (10) into (7b), we have

$$\dot{\boldsymbol{e}}_{\boldsymbol{d\eta}} = -\boldsymbol{k}_{\boldsymbol{\eta}}\boldsymbol{K}(\boldsymbol{e}_{\boldsymbol{d\eta}}) + \boldsymbol{J}_{\boldsymbol{u}}{}^{-1}\boldsymbol{\zeta}_{\boldsymbol{\eta}}. \tag{13}$$

**Theorem 1.** *For the subsystem (2b), with the control input $\boldsymbol{\tau}_{\boldsymbol{\eta}}$ designed as in (10), the zero equilibrium of the errors $\boldsymbol{e}_{\boldsymbol{\eta}}$, $\boldsymbol{e}_{\boldsymbol{d\eta}}$, and $\boldsymbol{\zeta}_{\boldsymbol{\eta}}$ of the closed-loop will converge to a bounded region ultimately.*

**Proof.** Define a nonnegative Lyapunov function $V_{\zeta_\eta} \in \mathbb{R}$ as follows:

$$V_{\zeta_\eta}(\zeta_\eta) = \frac{1}{2}\zeta_\eta^\top \rho_\eta^{-1}\zeta_\eta.$$

Considering the symmetry of the matrix $\boldsymbol{J}_u$ and substituting (12) into the time derivative of $V_{\zeta_\eta}$, we have

$$\begin{aligned}\dot{V}_{\zeta_\eta} &= \zeta_\eta^\top \rho_\eta^{-1}\dot{\zeta}_\eta \\ &= -\zeta_\eta^\top \boldsymbol{J}_u{}^{-1}\frac{\partial \boldsymbol{K}(\boldsymbol{e}_{d\eta})}{\partial \boldsymbol{e}_{d\eta}}\boldsymbol{J}_u{}^{-1}\zeta_\eta - \zeta_\eta^\top \rho_\eta^{-1}(\mathrm{sgn}(\zeta_\eta)\circ\bar{\tau}_{ds}) - \zeta_\eta^\top \rho_\eta^{-1}\dot{\tau}_s \\ &\le -(\boldsymbol{J}_u{}^{-1}\zeta_\eta)^\top \boldsymbol{J}_u{}^{-1}\zeta_\eta \le 0. \end{aligned} \tag{14}$$

Then, the equilibrium of the estimation error $\zeta_\eta$ is asymptotically stable, and the RISE-based adaptive law $\hat{\tau}_s + \beta_\eta$ can converge to its true value $\tau_s$ theoretically.

Following the aforementioned conclusion, define a Lyapunov function $V_\eta \in \mathbb{R}$ as follows:

$$V_\eta(\boldsymbol{e}_{d\eta}, \zeta_\eta) = \frac{1}{2}\boldsymbol{K}(\boldsymbol{e}_{d\eta})^\top \boldsymbol{K}(\boldsymbol{e}_{d\eta}) + \frac{1}{2}\zeta_\eta^\top \rho_\eta^{-1}\boldsymbol{k}_\eta^{-1}\zeta_\eta. \tag{15}$$

Substituting (12), (13), and (14) into the time derivative of (15) yields

$$\begin{aligned}\dot{V}_\eta &= \boldsymbol{K}(\boldsymbol{e}_{d\eta})^\top \frac{\partial \boldsymbol{K}(\boldsymbol{e}_{d\eta})}{\partial \boldsymbol{e}_{d\eta}}(-\boldsymbol{k}_\eta \boldsymbol{K}(\boldsymbol{e}_{d\eta}) + \boldsymbol{J}_u{}^{-1}\zeta_\eta) \\ &\quad - (\boldsymbol{J}_u{}^{-1}\zeta_\eta)^\top \boldsymbol{k}_\eta{}^{-1}\frac{\partial \boldsymbol{K}(\boldsymbol{e}_{d\eta})}{\partial \boldsymbol{e}_{d\eta}}\boldsymbol{J}_u{}^{-1}\zeta_\eta \\ &\le -\frac{1}{2}\boldsymbol{e}_{d\eta}{}^\top \boldsymbol{k}_\eta \boldsymbol{e}_{d\eta} - \frac{1}{2}(\boldsymbol{J}_u{}^{-1}\zeta_\eta)^\top \boldsymbol{k}_\eta{}^{-1}\boldsymbol{J}_u{}^{-1}\zeta_\eta \\ &\le -\frac{\lambda_\eta}{2}\|[\boldsymbol{e}_{d\eta}{}^\top \ (\boldsymbol{J}_u{}^{-1}\zeta_\eta)^\top]^\top\|^2 \le 0, \end{aligned}$$

where $\lambda_\eta = \lambda_{min}\left(\mathrm{diag}(\boldsymbol{k}_\eta, \boldsymbol{k}_\eta{}^{-1})\right)$, and $\lambda_{min}(\cdot)$ denotes the smallest eigenvalue of a matrix.

Consequently, the results in (14) and (26) imply that both the estimation error $\zeta_\eta$ and the state error $\boldsymbol{e}_{d\eta}$ of the inner closed-loop system (2b) and (13) are locally and asymptotically stable. Once $\boldsymbol{e}_{d\eta} = 0$, it follows from (6) that $\dot{\boldsymbol{e}}_\eta = -\boldsymbol{\alpha}_\eta \boldsymbol{e}_\eta$, and the error $\boldsymbol{e}_\eta$ is also locally and asymptotically stable.

### 4.3. Outer-loop controller

As demonstrated in Fig. 3, the outer-loop controller consists of both a velocity controller and a decoupler for managing the CTRUAV's velocity. In the manual mode of most flight control systems, speed control is required rather than position control. Additionally, speed control serves as the foundation for position control and trajectory tracking control. Therefore, this work primarily focuses on low-level velocity control for the CTRUAV.

#### 4.3.1. Velocity controller

The outer-loop velocity control law computes the desired thrust force $\boldsymbol{F}_{\xi d}$ for (3) to enable the CTRUAV to track the target velocity $\dot{\boldsymbol{\xi}}_{\boldsymbol{d}}$. Subsequently, the I&I-based adaptive velocity controller is presented as follows.

Define the velocity error as

$$\boldsymbol{e}_{\dot{\xi}} = [e_{\dot{x}}\ e_{\dot{y}}\ e_{\dot{z}}]^\top = \dot{\boldsymbol{\xi}}_{\boldsymbol{d}} - \dot{\boldsymbol{\xi}}, \tag{16}$$

After substituting (2a) into the time derivative of (16), it is obtained that

$$\dot{\boldsymbol{e}}_{\dot{\xi}} = -m^{-1}\left(\boldsymbol{F}_\xi + \boldsymbol{F}_s\right) + \boldsymbol{\gamma}_\xi, \tag{17}$$

with $\boldsymbol{\gamma}_\xi = \ddot{\boldsymbol{\xi}}_{\boldsymbol{d}} - m^{-1}(m\boldsymbol{g} + \boldsymbol{R}_b^i \boldsymbol{D}_{\xi b})$.

Let the estimation error $\zeta_\xi$ be defined as

$$\zeta_\xi = \hat{\boldsymbol{F}}_s + \beta_\xi(\boldsymbol{e}_{\dot{\xi}}) - \boldsymbol{F}_s, \tag{18}$$

where $\hat{\boldsymbol{F}}_s$ is the estimation of the unknown disturbance force $\boldsymbol{F}_s$ with bounded time derivative, and $\boldsymbol{\beta}_\xi = [\beta_x\ \beta_y\ \beta_z]^\top$ represents a continuous vector function that will be designed subsequently. Differentiating (18) with respect to time yields

$$\dot{\zeta}_\xi = \dot{\hat{\boldsymbol{F}}}_s + \frac{\partial \boldsymbol{\beta}_\xi}{\boldsymbol{e}_{\dot{\xi}}}\dot{\boldsymbol{e}}_{\dot{\xi}} - \dot{\boldsymbol{F}}_s. \tag{19}$$

Based on (19), the desired control force $\boldsymbol{F}_{\xi d}$ is designed as

$$\boldsymbol{F}_{\xi d} = m\boldsymbol{k}_\xi \boldsymbol{K}(\boldsymbol{e}_{\dot{\xi}}) - (\hat{\boldsymbol{F}}_s + \boldsymbol{\beta}_\xi) + m\boldsymbol{\gamma}_\xi, \tag{20}$$

with the RISE-based adaptive update law

$$\dot{\hat{\boldsymbol{F}}}_s = \frac{\partial \boldsymbol{\beta}_\xi}{\partial \boldsymbol{e}_{\dot{\xi}}}\left(m^{-1}\left(\boldsymbol{F}_\xi + \hat{\boldsymbol{F}}_s + \boldsymbol{\beta}_\xi\right) - \boldsymbol{\gamma}_\xi\right) - \mathrm{sgn}(\zeta_\xi)\circ\bar{\boldsymbol{F}}_{\boldsymbol{ds}}, \tag{21a}$$

$$\boldsymbol{\beta}_\xi = -\rho_\xi m^{-1}\boldsymbol{K}(\boldsymbol{e}_{\dot{\xi}}), \tag{21b}$$

where $\boldsymbol{k}_\xi = \mathrm{diag}(k_x, k_y, k_z)$ and $\boldsymbol{\rho}_\xi = \mathrm{diag}(\rho_x, \rho_y, \rho_z)$ are both diagonal positive-definite matrices. According to the velocity model (2a), we define

$$\boldsymbol{F}_{\boldsymbol{sr}} = m\ddot{\boldsymbol{\xi}} - \boldsymbol{F}_{\xi r} - m\boldsymbol{g} - \boldsymbol{R}_b^i \boldsymbol{D}_{\xi b},$$

which is treated as the actual disturbance $\boldsymbol{F}_s$ in the adaptive law, and the term $\boldsymbol{F}_{\xi r}$ is the actual thrust force in the body frame $\mathscr{B}$ and calculated as

$$\boldsymbol{F}_{\xi r} = \boldsymbol{R}_{dr}[F_{xb}\ F_{zb}]^\top,$$

where $F_{xb}$ and $F_{zb}$ are given in (28), and $\boldsymbol{R}_{dr} = \boldsymbol{R}_b^i \begin{bmatrix}1 & 0 & 0\\ 0 & 0 & 1\end{bmatrix}^\top$. Then, the term $\zeta_\xi$ in (21a) is obtained as $\zeta_\xi = \hat{\boldsymbol{F}}_s + \boldsymbol{\beta}_\xi - \boldsymbol{F}_{sr}$.

Setting the control force $\boldsymbol{F}_\xi$ in (17) as $\boldsymbol{F}_{\xi d}$ in (20). By substituting (18) and (20) into (17), we have

$$\dot{\boldsymbol{e}}_{\dot{\xi}} = -\boldsymbol{k}_\xi \boldsymbol{K}(\boldsymbol{e}_{\dot{\xi}}) + m^{-1}\zeta_\xi. \tag{22}$$

Substituting (20), (21) and (22) into (19) yields

$$\dot{\zeta}_\xi = -\rho_\xi m^{-2}\frac{\partial \boldsymbol{K}(\boldsymbol{e}_{\dot{\xi}})}{\partial \boldsymbol{e}_{\dot{\xi}}}\zeta_\xi - \mathrm{sgn}(\zeta_\xi)\circ\bar{\boldsymbol{F}}_{\boldsymbol{ds}} - \dot{\boldsymbol{F}}_s. \tag{23}$$

**Theorem 2.** *For the subsystem (2a), if the control input $\boldsymbol{F}_\xi$ is designed as $\boldsymbol{F}_{\xi d}$ in (20), the errors $\boldsymbol{e}_{\dot{\xi}}$ and $\zeta_\xi$ will converge to a bounded region ultimately.*

**Proof.** Define the Lyapunov function as follows:

$$V_{\zeta_\xi} = \frac{1}{2}\zeta_\xi^\top \rho_\xi^{-1}\zeta_\xi. \tag{24}$$

Substituting (23) into the time derivative of (24) yields

$$\begin{aligned}\dot{V}_{\zeta_\xi} &= \zeta_\xi^\top \rho_\xi^{-1}\dot{\zeta}_\xi \\ &= -m^{-2}\zeta_\xi^\top \frac{\partial \boldsymbol{K}(\boldsymbol{e}_{\dot{\xi}})}{\partial \boldsymbol{e}_{\dot{\xi}}}\zeta_\xi - \zeta_\xi^\top \rho_\xi^{-1}\mathrm{sgn}(\zeta_\xi)\circ\bar{\boldsymbol{F}}_{\boldsymbol{ds}} - \zeta_\xi^\top \rho_\xi^{-1}\dot{\boldsymbol{F}}_s \\ &\le -m^{-2}\zeta_\xi^\top \zeta_\xi \le 0. \end{aligned} \tag{25}$$

Then, the estimation error $\zeta_\xi$ is locally asymptotically stable. Define a Lyapunov candidate $V_\xi \in \mathbb{R}$ as follows:

$$V_\xi(\boldsymbol{e}_{\dot{\xi}}, \zeta_\xi) = \frac{1}{2}\boldsymbol{K}(\boldsymbol{e}_{\dot{\xi}})^\top \boldsymbol{K}(\boldsymbol{e}_{\dot{\xi}}) + \frac{1}{2}\zeta_\xi^\top \rho_\xi^{-1}\boldsymbol{k}_\xi^{-1}\zeta_\xi.$$

By taking the time derivative of $V_\xi$ and substituting (23) and (22) into the derived equation, we have

$$\dot{V}_\xi = \boldsymbol{K}(\boldsymbol{e}_{\dot{\xi}})^\top \frac{\partial \boldsymbol{K}(\boldsymbol{e}_{\dot{\xi}})}{\partial \boldsymbol{e}_{\dot{\xi}}} \left(-\boldsymbol{k}_\xi \boldsymbol{K}(\boldsymbol{e}_{\dot{\xi}}) + m^{-1}\boldsymbol{\zeta}_\xi\right) - \boldsymbol{\zeta}_\xi^\top \boldsymbol{k}_\xi^{-1} m^{-2} \frac{\partial \boldsymbol{K}(\boldsymbol{e}_{\dot{\xi}})}{\partial \boldsymbol{e}_{\dot{\xi}}} \boldsymbol{\zeta}_\xi$$
$$\leq -\frac{1}{2}\boldsymbol{e}_{\dot{\xi}}^\top \boldsymbol{k}_\xi \boldsymbol{e}_{\dot{\xi}} - \frac{1}{2} m^{-2} \boldsymbol{\zeta}_\xi^\top \boldsymbol{k}_\xi^{-1} \boldsymbol{\zeta}_\xi \leq 0. \tag{26}$$

Consequently, the results in (25) and (26) indicate that the estimation error $\boldsymbol{\zeta}_\xi$ and the state error $\boldsymbol{e}_{\dot{\xi}}$ of the closed-loop system (2a) and (20) are locally and asymptotically stable.

#### 4.3.2. Decoupler

The outer-loop decoupler is utilized to convert the desired resultant force $F_{\xi d}$, derived from the velocity control, into the target roll angle $\phi_d$ and the thrust force $\boldsymbol{F}_{\boldsymbol{xzb}} = [F_{xb}\ F_{zb}]^\top$ of the rotors in the body-fixed frame. As indicated in (3), the relationship between $\phi_d$, $\boldsymbol{F}_{\boldsymbol{xzb}}$, and $\boldsymbol{F}_{\xi d}$ is described by the equation below:

$$\boldsymbol{F}_{\xi d} = \boldsymbol{R}_d \boldsymbol{F}_{\boldsymbol{xzb}}, \tag{27}$$

where

$$\boldsymbol{R}_d = \begin{bmatrix} c\psi & -s\psi & 0 \\ s\psi & c\psi & 0 \\ 0 & 0 & 1 \end{bmatrix} \begin{bmatrix} c\theta & 0 & s\theta \\ 0 & 1 & 0 \\ -s\theta & 0 & c\theta \end{bmatrix} \begin{bmatrix} 1 & 0 & 0 \\ 0 & c\phi_d & -s\phi_d \\ 0 & s\phi_d & c\phi_d \end{bmatrix} \begin{bmatrix} 1 & 0 \\ 0 & 0 \\ 0 & 1 \end{bmatrix}.$$

Subsequently, $F_{xb}$, $F_{zb}$, and $\phi_d$ can be obtained as follows:

$$\phi_d = \arctan\left(\frac{F_{xd}s\psi - F_{yd}c\psi}{F_{xd}s\theta c\psi + F_{yd}s\theta s\psi + F_{zd}c\theta}\right), \tag{28a}$$

$$F_{xb} = F_{xd}c\theta c\psi + F_{yd}c\theta s\psi - F_{zd}s\theta, \tag{28b}$$

$$F_{zb} = \frac{F_{xd}s\theta c\psi + F_{yd}s\theta s\psi + F_{zd}c\theta}{c\phi_d}. \tag{28c}$$

Considering the constraints specified in (1) and the operational mechanics of the CTRUAV's rotors, it is determined that $F_{zb} \leq 0$. Therefore, in the scenario where $F_{xd}s\theta c\psi + F_{yd}s\theta s\psi + F_{zd}c\theta = 0$, $\phi_d$ is set as follows to avoid singularity:

$$\phi_d = \begin{cases} b_\phi, & F_{xd}s\psi - F_{yd}c\psi > 0, \\ -b_\phi, & F_{xd}s\psi - F_{yd}c\psi < 0, \\ \phi, & F_{xd}s\psi - F_{yd}c\psi = 0, \end{cases}$$

where $b_\phi$ is a designed positive value less than $\pi/2$.

**Remark 3.** Although the control strategy in [24] possesses motion control capability, it cannot theoretically estimate disturbance values. By the proposed I&I-based adaptive law, the disturbance estimations $\hat{\boldsymbol{\tau}}_s$ and $\hat{\boldsymbol{F}}_s$ can theoretically converge to their actual values without the need for additional sensors. Consequently, the I&I controller offers superior performance in terms of transient response and disturbance estimation, which will be further verified in the following experiments.

## 5. Experiments

A CTRUAV is constructed to demonstrate the performance and efficacy of the proposed control strategy. Each CTR module is equipped with a pair of AEO CRM2208 1600KV coaxial motors, two AEO 8040 propellers rotating in opposite directions, two FLYCOLOR Fairy 20-Amp Electronic Speed Controllers (ESCs), and an EMAX ES3005 servo. The tail rotor module includes a FLYCOLOR Fairy 20-Amp ESC, a SUNNYSKY X2208 1500KV motor, and an AEO 8040 propeller. The flight control hardware system is constructed based on a TM4C123G MPU, which is a 32-bit ARM Cortex-M4F microcontroller with a maximum operating frequency of 80 MHz and equipped with a Floating Point Unit (FPU) for efficient processing of the proposed control algorithm. The refresh rates of the mixer, the inner-loop controller, and the outer-loop controller are set to 500 Hz, 500 Hz, and 100 Hz, respectively. The velocity and altitude are measured using optical flow and laser sensors, respectively. Given the relatively limited research on the CTRUAV control, we have, for the time being, compared the proposed control strategy with the conventional I&I-based adaptive controller without segmented gains and the existing adaptive controller [24] in experiments. The superiority of the adaptive attitude controller over a controller that integrates PD terms and feedforwards has already been validated in [24]. In this work, the Ziegler-Nichols Tuning Rule [5] is employed to adjust the control parameters. The control parameters of the proposed controller are listed in Table 1. In the proposed I&I-based adaptive control strategy, the functions $\boldsymbol{K}(\boldsymbol{e}_{\dot{\xi}})$ and $\boldsymbol{K}(\boldsymbol{e}_{d\eta})$ are designed to further improve the control performance and make the control law design for (10) and (20) more flexible. In the experiments, the function $\mathscr{K}(x)$ in $\boldsymbol{K}(\cdot)$ is chosen as follows:

**Table 1**
Control parameters of the proposed controller.

| Attitude control parameters | Value |
|---|---|
| $\alpha_\phi,\ \alpha_\theta,\ \alpha_\psi$ | 6.8, 6.2, 5.5 |
| $k_\phi,\ k_\theta,\ k_\psi$ | 34, 32, 5.5 |
| $\rho_\phi,\ \rho_\theta,\ \rho_\psi$ | 1.2, 1.3, 0.06 |
| **Velocity control parameters** | **Value** |
| $k_x,\ k_y,\ k_z,$ | 3.8, 2.4, 2 |
| $\rho_x,\ \rho_y,\ \rho_z$ | 0.8, 0.64, 0.6 |

$$\mathscr{K}(x) = \begin{cases} x + a - a^{2/5}, & x < -a, \\ \frac{x - x_i}{x_{i+1} - x_i}\left(x_{i+1}^{(2/5)} - x_i^{(2/5)}\right) + x_i^{(2/5)}, & x_i \leq x < x_{i+1}, \\ x - a + a^{2/5}, & x \geq a, \end{cases}$$

where $a = \frac{2}{5}^{5/3}$, $x_i = \frac{i}{N}a$, $i = -N, \ldots, -1,\ 0,\ 1, \ldots, N-1$, and $x_i^{(p/q)} = \text{sign}(x_i)|x_i|^{p/q}$, with positive integers $q$ and $p$.

The coefficients $c_{fu}$ and $c_{fd}$ in (4) differ due to the influence of the rotor downwash flows between the upper rotor and the lower rotor. To determine these coefficients, it is necessary to construct the thrust and reaction torque model of the CTR modules. The relationships between $F_r$, $F_l$, $\tau_r$, $\tau_l$, and the PWM signals $P_i$ (1050 μs ∼ 1950 μs) to the electronic speed controllers of the rotors $i$ are expressed as $F_r = F_c(P_4, P_1)$, $F_l = F_c(P_2, P_3)$ $\tau_r = \tau_c(P_4, P_1)$, and $\tau_l = -\tau_c(P_2, P_3)$, where $F_c$ and $\tau_c$ are the models of the thrust and reaction torque of the CTR module, respectively. The experimental platforms are shown in Fig. 4. Quadratic fitting surfaces are used to model the performance of the CTR modules as described below:

$$F_c(P_u, P_d) = c_{tu}(P_u - 1050)^2 + c_{td}(P_d - 1050)^2,$$
$$\tau_c(P_u, P_d) = c_{ru}(P_u - 1050)^2 - c_{rd}(P_d - 1050)^2.$$

According to the measurement results in Fig. 4c, we have $c_{tu} = 0.8402 \times 10^{-5}$, $c_{td} = 1.059 \times 10^{-5}$, $c_{ru} = 1.024 \times 10^{-7}$, and $c_{rd} = 0.9325 \times 10^{-7}$. Then, the coefficients $c_{fu}$ and $c_{fd}$ in (4) are obtained by $c_{fu} = c_{ru}/c_{tu}$, $c_{fd} = c_{rd}/c_{td}$. It should be noted that the aforementioned coefficients of the rotors were obtained on a fixed platform on the ground, without considering the effects of airspeed. Additionally, the support structure of the test platform partially blocks the rotor wake. Therefore, correction factors need to be added and adjusted based on the results of actual flight tests. Subsequently, key physical parameters of the CTRUAV, such as mass, rotational inertia, and rotor coefficients, are listed in Table 2.

1) Ground Bench Test: With the proposed I&I-based adaptive controller, conventional I&I-based adaptive controller, and the adaptive controller in [24], the CTRUAV tracks desired attitudes on a ground bench. In the first two cases for attitude tracking of $\phi$ and $\theta$, a 200 g

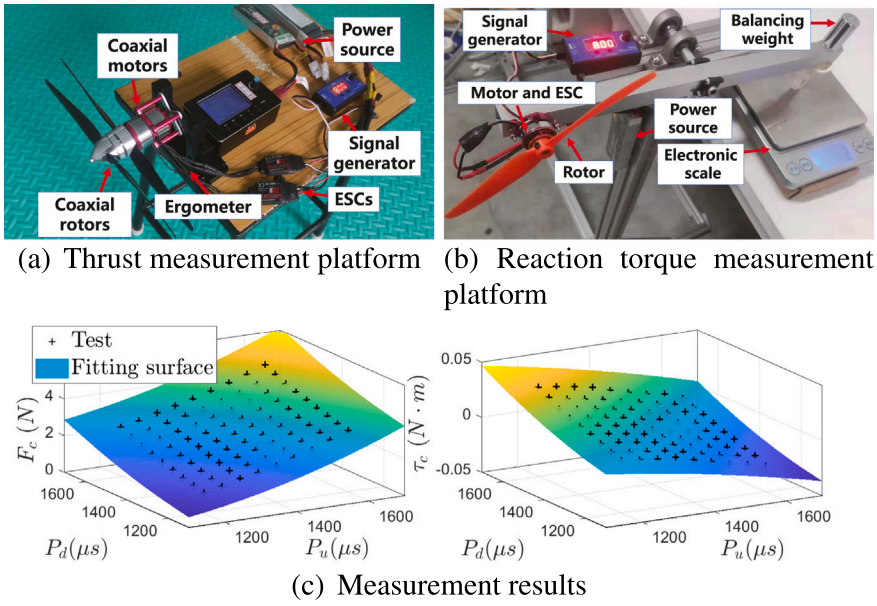


(a) Thrust measurement platform (b) Reaction torque measurement platform

(c) Measurement results

**Fig. 4.** Measurement of the CTR module.

**Table 2**
Physical parameters.

| Parameter | Description | Value | Unit |
|---|---|---|---|
| $g$ | Gravity | 9.807 | m/s$^2$ |
| $m$ | Mass | 1.19 | kg |
| $l_f\ l_b\ l_s$ | Distance | 0.085 0.245 0.131 | m |
| $I_x\ I_y\ I_z$ | Inertia tensor | 10.11 8.99 17.3 | g · m$^2$ |
| $c_{fu}$ | Coefficient | $1.219 \times 10^{-2}$ | – |
| $c_{fd}$ | Coefficient | $0.881 \times 10^{-2}$ | – |
| $c_b$ | Coefficient | $1.382 \times 10^{-2}$ | – |

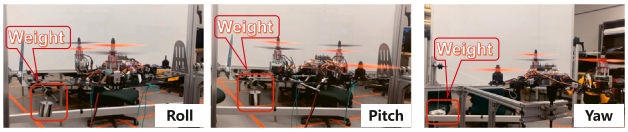


**Fig. 5.** Snapshots of ground bench test.

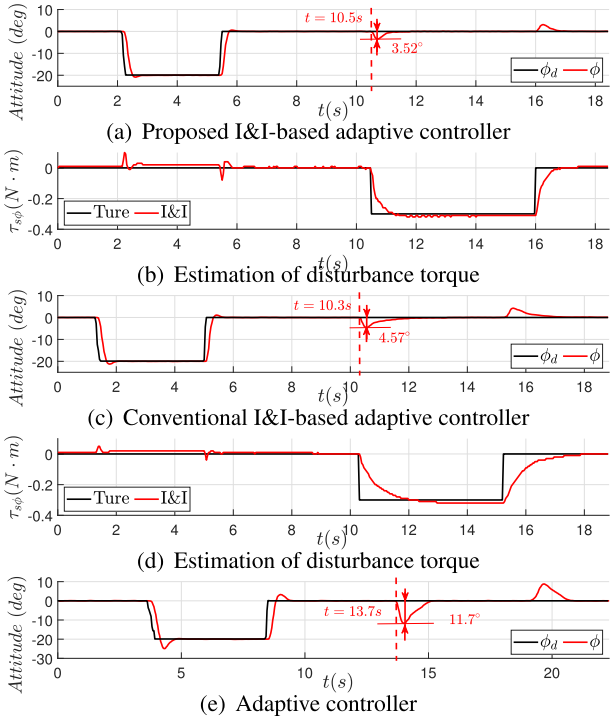


(a) Proposed I&I-based adaptive controller

(b) Estimation of disturbance torque

(c) Conventional I&I-based adaptive controller

(d) Estimation of disturbance torque

(e) Adaptive controller

**Fig. 6.** Experimental results of attitude tracking for $\phi$.

weight is suspended on a carbon fiber rod with length of 0.15 m to generate torques $\boldsymbol{\tau}_s = [-0.3\ 0\ 0]^\top$ (N · m) and $\boldsymbol{\tau}_s = [0\ 0.3\ 0]^\top$ (N · m), respectively. In the third case, a 75 g weight is suspended on the tail of the CTRUAV to produce a disturbance torque $\boldsymbol{\tau}_s = [0\ 0\ 0.15]^\top$ (N · m). In the these tests, the CTRUAV will track the desired attitude with the same fixed tilt angles $\alpha_r = \alpha_l = 0°$. Hence, this effectively addresses the internal cancellation problem in [19,24] by the proposed mixer.

Snapshots of the tests are depicted in Fig. 5. A video of the ground bench test is available at https://youtu.be/-puC8TEs5p8.

According to the results in Fig. 6, 7, 8, and Table 3, the designed controller demonstrates a significant improvement in the transient performance and anti-interference capability in the presence of external torques. For instance, the settling time of the proposed improved I&I-based adaptive controller is only 0.32 s in direction $\phi$, which is 5.9 % and 37.2 % shorter than those of the conventional I&I-based adaptive controller and the adaptive controller, respectively. Influenced by the external torque produced by the weight, the maximum error of the proposed controller is only 3.49°, which is 18.3 % less than 4.27° of the conventional I&I-based adaptive controller and 41.7 % less than 5.99° of the adaptive controller in direction $\theta$. Furthermore, the RMSE of the designed controller is only 0.93° and 11.4 % less than 1.05° of the conventional I&I-based adaptive controller and 80.9 % less than 4.87° of the adaptive controller in direction $\psi$. Furthermore, according to the results in Fig. 6a, 6c, 7b, 7d, 8b, and 8d, The I&I-based adaptive laws can converge to their true values, which is consistent with the theoretical results presented in Theorem 1. Furthermore, the estimated values of the proposed method with segmented gains converge faster than those of the conventional I&I-based method, as clearly demonstrated in Fig. 6a, 6c, 7b, and 7d.

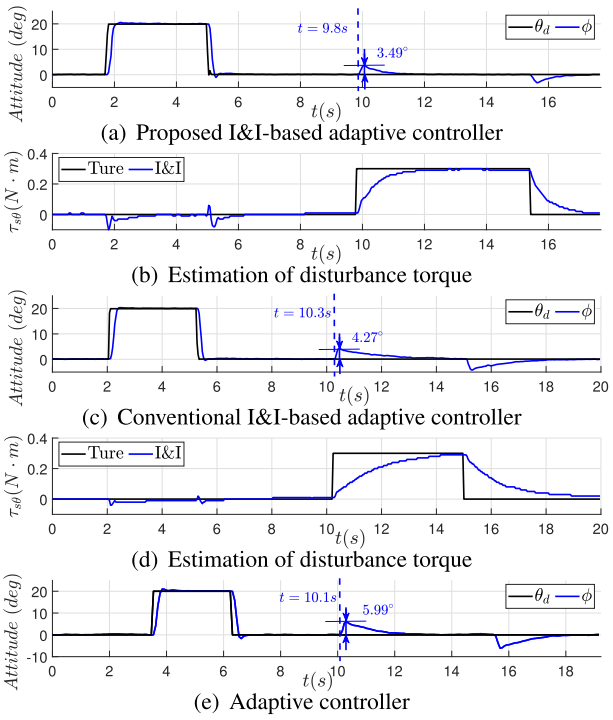


**Fig. 7.** Experimental results of attitude tracking for $\theta$.

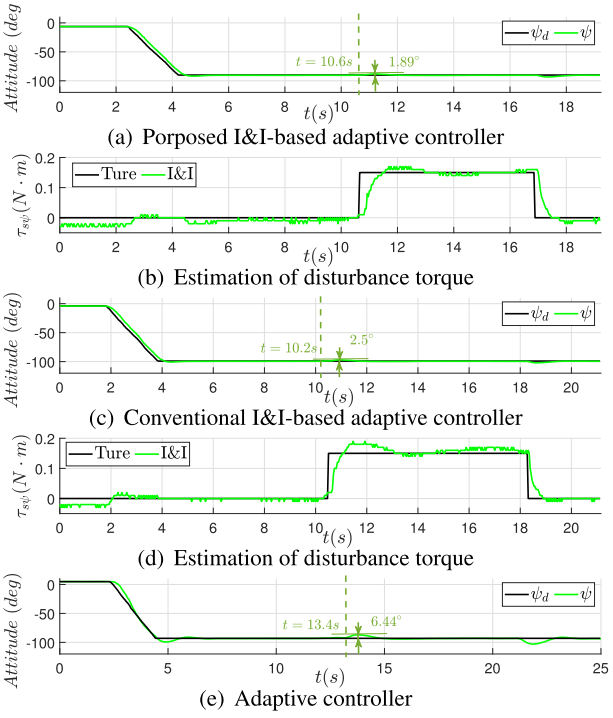


**Fig. 8.** Experimental results of attitude tracking for $\psi$.

It should be noted that in contrast to the mixer in [19,24], the tilt angles of the CTR modules are set identically in the proposed mixer. Consequently, the internal force cancellation problem, which is evident based on the principle of force composition, is resolved.

**Table 3**
Comparison of experimental results.

| | Settling time(s) | Maximum error (° or $m/s$) | RMSE (° or $m/s$) |
|---|---|---|---|
| | Designed | | |
| $\phi$ | 0.32(5.9% ↓) | 3.52°(17.6% ↓) | 1.2°(38.7% ↓) |
| $\theta$ | 0.3(3.5% ↓) | 3.49°(18.3% ↓) | 1.33°(45.5% ↓) |
| $\psi$ | 1.95(22.3% ↓) | 1.89°(24.4% ↓) | 0.93°(11.4% ↓) |
| | Conventional I&I | | |
| $\phi$ | 0.34 | 4.57° | 1.96° |
| $\theta$ | 0.34 | 4.27° | 2.44° |
| $\psi$ | 2.53 | 2.5° | 1.05° |
| | Adaptive | | |
| $\phi$ | 0.51 | 11.7° | 5.61° |
| $\theta$ | 0.31 | 5.99° | 3.17° |
| $\psi$ | 2.85 | 6.44° | 4.87° |
| | Designed | | |
| $\dot{x}$ | 1.23(20.1% ↓) | 0.18$m/s$(30.8% ↓) | 0.107$m/s$(23.6% ↓) |
| $\dot{y}$ | 1.19(20.7% ↓) | 0.18$m/s$(21.7% ↓) | 0.083$m/s$(41.5% ↓) |
| $\dot{z}$ | – | 0.23$m/s$(8% ↓) | 0.117$m/s$(25% ↓) |
| | Conventional I&I | | |
| $\dot{x}$ | 1.54 | 0.26$m/s$ | 0.14$m/s$ |
| $\dot{y}$ | 1.5 | 0.23$m/s$ | 0.142$m/s$ |
| $\dot{z}$ | – | 0.25$m/s$ | 0.156$m/s$ |
| | Adaptive | | |
| $\dot{x}$ | 1.69 | 0.3$m/s$ | 0.215$m/s$ |
| $\dot{y}$ | 1.69 | 0.31$m/s$ | 0.22$m/s$ |
| $\dot{z}$ | – | 0.26$m/s$ | 0.135$m/s$ |

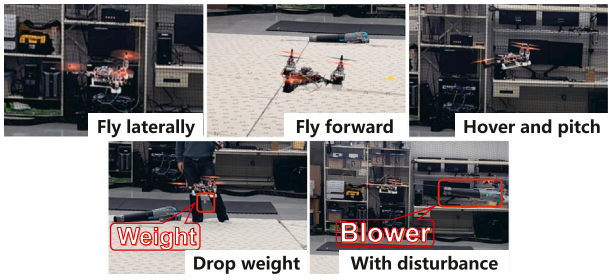


**Fig. 9.** Snapshots of ground bench test.

2) Flight Test: Controlled by different controllers, the CTRUAV tracks desired velocity and attitude under external disturbances. The CTRUAV firstly takes off and moves laterally at the speed of $\dot{y}_d = 2$ m/s, and changes its yaw direction to fly forward at desired velocity $\dot{x}_d = 2$ m/s. Then, the CTRUAV pitches up its head with an attitude of $\theta_d = 15°$, At last, to assess control performance under disturbance, airflow perturbations generated by the blower is applied to the CTRUAV, and a weight of 200 g is suspended on the bottom of the CTRUAV. To increase the consistency of the external disturbance, the blower is placed in the same relative position as possible. Snapshots of the flight test are presented in Fig. 9. A video of the real flight test can be viewed at https://youtu.be/WB87WawTXSQ.

Based on the results, the controllers successfully track the desired velocity and attitude during the real flight process. Compared with the adaptive controller in [24], the designed I&I-based adaptive controller shows obvious improvement in transient performance, control accuracy, and steady-state performance. According to the results in Fig. 10a, 11a,

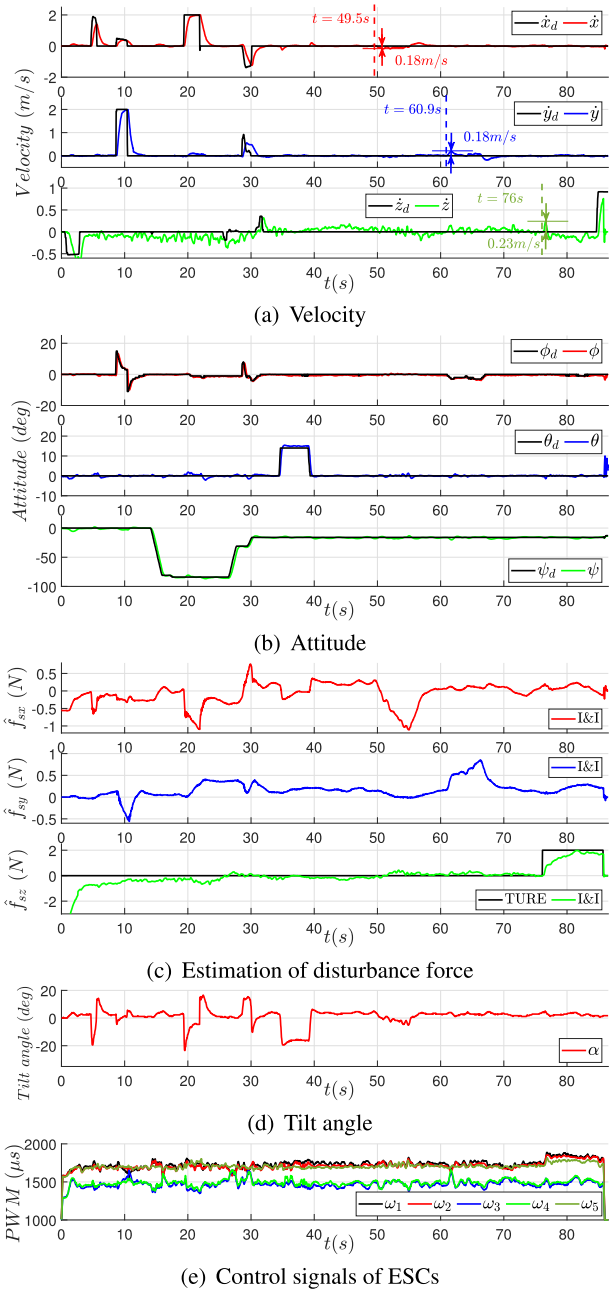


**Fig. 10.** Experimental results of real flight with the proposed I&I-based adaptive controller.

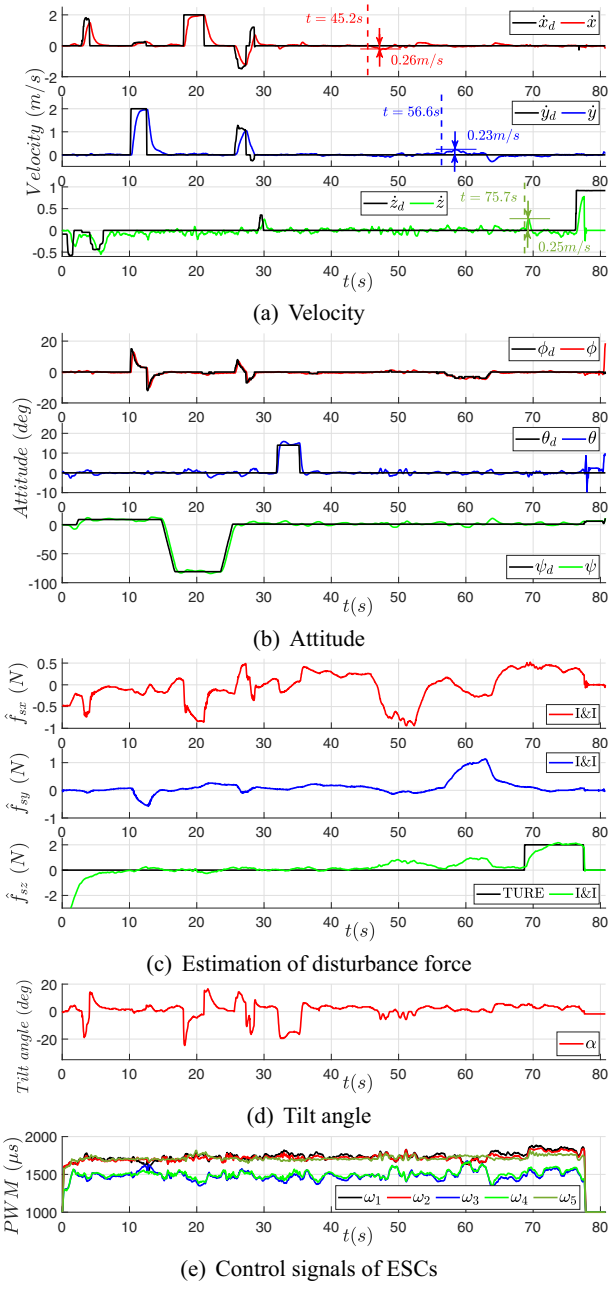


**Fig. 11.** Experimental results of real flight with the conventional I&I-based adaptive controller.

12a, and Table 3, the settling time is only 1.23 s with the proposed controller, which is 20.1 % shorter than 1.54 s of the conventional I&I-based adaptive controller and 27.2 % less than 1.69 s of the adaptive controller in direction $\dot{x}$. The maximum error of the I&I-based adaptive controller in the presence of the external disturbance is only 0.18 m/s and 21.7 % less than 0.23 m/s of the conventional I&I-based adaptive controller and 41.9 % less than 0.31 m/s of the adaptive controller in direction $\dot{y}$. Additionally, the RMSE of the proposed controller is 0.117 m/s and 25 % of 0.156 m/s of the conventional I&I-based adaptive controller and 13.3 % less than 0.135 m/s of the adaptive controller in direction $\dot{z}$. According to Fig. 10b, 11b, and 12b, the proposed inner-loop controller and the conventional I&I-based adaptive attitude controller can track the given step signals $\phi_d$ produced by the outer-loop controllers and the desired attitude $\theta_d$ and $\psi_d$, achieving better control accuracy. Furthermore, the estimations of disturbance forces can eventually converge to their true values with the I&I-based adaptive update law, which is not applicable to the adaptive controller in [24].

Therefore, compared to the conventional I&I-based adaptive attitude controller and the adaptive controller, the proposed method improves the convergence speed, disturbance-rejection capability, and the stability of the CTRUAV. Moreover, the designed I&I-based adaptive update law enables rapid and accurate estimation of the disturbance torque and force. Additionally, with the mixer, the CTRUAV's attitude can be controlled using identical right and left tilt angles, effectively resolving the inefficient internal force cancellation problem in existing CTRUAV's mixer.

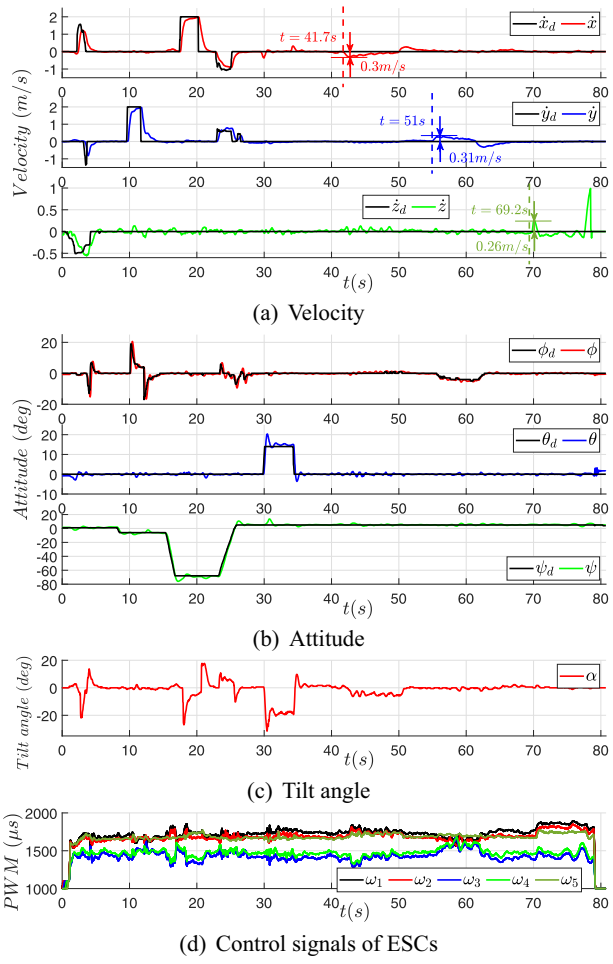


**Fig. 12.** Experimental results of real flight with adaptive controller.

## 6. Conclusion

This work proposes an RISE-based I&I adaptive motion controller for a CTRUAV under external disturbances. In the controller design, the RISE-based I&I adaptive methodology is employed to design the inner-loop and outer-loop control algorithms, enabling the estimation and compensation of time-varying disturbance torques and forces. The stability of the closed-loop system is proven by Lyapunov method. The performance and superiority of the proposed controller are demonstrated through experiments. The results show that the proposed controller can achieve asymptotic tracking of the velocity and attitude reference trajectory while accurately estimating the disturbance torques and forces. However, the proposed control system has some limitations: It does not account for the component failures or the singularity problem of the Euler angles.

## Acknowledgements

This work was partially supported in part by the National Natural Science Foundation of China under grants Nos. 62203086, 62173062, and 62206040, and by the Fundamental ResearchFunds for the Central Universities under Grant 044420250104. We would like to thank Alan Lynch for providing the flight test site.

## CRediT authorship contribution statement

**Longlong Chen:** Writing – original draft. **Yanmei Jia:** Writing – review & editing. **Sihao Sun:** Writing – review & editing, Data curation. **Zongyang Lv:** Supervision. **Yuhu Wu:** Supervision, Funding acquisition.

## Declaration of competing interest

The authors declare that they have no known competing financial interests or personal relationships that could have appeared to influence the work reported in this paper.

## References

[1] Astolfi A, Karagiannis D, Ortega R. Nonlinear and adaptive control with applications, vol. 187. Springer; 2008.
[2] Astolfi A, Ortega R. Immersion and invariance: a new tool for stabilization and adaptive control of nonlinear systems. IEEE Trans Autom Control 2003;48(4):590–606.
[3] Batrakov A. Mathematical model of the fuselage of a promising high-speed helicopter. Russ Aeronaut 2021;64(2):360–63.
[4] Beard R. Quadrotor dynamics and control rev 0.1. 2008.
[5] Bobál V. Technical note self-tuning ziegler-nichols pid controller. Int J Adapt Control Signal Process 1995;9(2):213–26.
[6] Chen C, Zhang J, Wang N, Shen L, Li Y. Conversion control of a tilt tri-rotor unmanned aerial vehicle with modeling uncertainty. Int J Adv Rob Syst 2021;18(4):17298814211027033.
[7] Chen L, Lv Z, Shen X, Wu Y, Sun XM. Adaptive attitude control for a coaxial tilt-rotor UAV via immersion and invariance methodology. IEEE/CAA J Autom Sinica 2022;9(9):1710–13.
[8] Chen L, Xiao J, Zheng Y, Alagappan NA, Feroskhan M. Design, modeling, and control of a coaxial drone. IEEE Trans Robot 2024;40:1650–63. https://doi.org/10.1109/TRO.2024.3354161
[9] D'Amato E, Di Francesco G, Notaro I, Tartaglione G, Mattei M. Nonlinear dynamic inversion and neural networks for a tilt tri-rotor UAV. IFAC-PapersOnLine 2015;48(9):162–67. https://doi.org/10.1016/j.ifacol.2015.08.077. 1st IFAC workshop on advanced control and navigation for autonomous aerospace vehicles ACNAAV'15. https://www.sciencedirect.com/science/article/pii/S2405896315009441
[10] D'Amato E, Di Francesco G, Notaro I, Tartaglione G, Mattei M. Nonlinear dynamic inversion and neural networks for a tilt tri-rotor UAV. IFAC-PapersOnLine 2015;48(9):162–67.
[11] Dydek ZT, Annaswamy AM, Lavretsky E. Adaptive control of quadrotor UAVs: a design trade study with flight evaluations. IEEE Trans Control Syst Technol 2013;21(4):1400–06.
[12] Elfeky M, Elshafei M, Saif AWA, Al-Malki MF. Modeling and simulation of quadrotor UAV with tilting rotors. Int J Control Autom Syst 2016;14(4):1047–55.
[13] Fischer N, Bhasin S, Dixon WE. Nonlinear control of an autonomous underwater vehicle: a rise-based approach. In: Proceedings of the 2011 American control conference; IEEE; 2011. p. 3972–77.
[14] Han Q, Liu X. Robust I&I adaptive control for a class of quadrotors with disturbances. IEEE Access 2020;8:216519–28. https://doi.org/10.1109/ACCESS.2020.3041030
[15] Kamel M, Verling S, Elkhatib O, Sprecher C, Wulkop P, Taylor Z, et al. The voliro omniorientational hexacopter: an agile and maneuverable tiltable-rotor aerial vehicle. IEEE Robot Autom Mag 2018;25(4):34–44.
[16] Karagiannis D, Astolfi A. Adaptive state feedback design via immersion and invariance. In: 2007 European control conference (ECC); IEEE; 2007. p. 553–58.
[17] Kendoul F, Fantoni I, Lozano R. Modeling and control of a small autonomous aircraft having two tilting rotors. IEEE Trans Robot 2006;22(6):1297–302. https://doi.org/10.1109/TRO.2006.882956
[18] Kwon YM, Park JS, Wie SY, Kang HJ, Kim DH. Aeromechanics analyses of a modern lift-offset coaxial rotor in high-speed forward flight. Int J Aeronaut Space Sci 2021;22(2):338–51.
[19] Li S, Lv Z, Feng L, Wu Y, Li Y. Nonlinear cascade control for a new coaxial tilt-rotor uav. Int J Control Autom Syst 2022;20(9):2948–58.
[20] Liang X, Fang Y, Sun N, Lin H, Zhao X. Adaptive nonlinear hierarchical control for a rotorcraft transporting a cable-suspended payload. IEEE Trans Syst Man Cybern Syst 2021;51(7):4171–82. https://doi.org/10.1109/TSMC.2019.2931812
[21] Liang X, Lin H, Zhang P, Wu S, Sun N, Fang Y. A nonlinear control approach for aerial transportation systems with improved antiswing and positioning performance. IEEE Trans Autom Sci Eng 2020;18(4):2104–14.
[22] Lim JW, Mcalister KW, Johnson W. Hover performance correlation for full-scale and model-scale coaxial rotors. J Am Helicopter Soc 2009;54(3):67–80.
[23] Liu Z, He Y, Yang L, Han J. Control techniques of tilt rotor unmanned aerial vehicle systems: a review. Chin J Aeronaut 2017;30(1):135–48.
[24] Lv Z, Wu Y, Zhao Q, Sun XM. Design and control of a novel coaxial tilt-rotor UAV. IEEE Trans Ind Electron 2022;69(4):3810–21. https://doi.org/10.1109/TIE.2021.3075886
[25] Papachristos C, Alexis K, Tzes A. Efficient force exertion for aerial robotic manipulation: exploiting the thrust-vectoring authority of a tri-tiltrotor UAV. In: 2014 IEEE international conference on robotics and automation (ICRA); IEEE; 2014. p. 4500–05.
[26] Patre PM, MacKunis W, Kaiser K, Dixon WE. Asymptotic tracking for uncertain dynamic systems via a multilayer neural network feedforward and rise feedback control structure. IEEE Trans Autom Control 2008;53(9):2180–85.
[27] Rago C, Prasanth R, Mehra RK, Fortenbaugh R. Failure detection and identification and fault tolerant control using the IMM-KF with applications to the eagle-eye UAV. In: Proceedings of the 37th IEEE conference on decision and control (Cat. No. 98CH36171); IEEE; 1998. p. 4208–13.
[28] Romero A, Sun S, Foehn P, Scaramuzza D. Model predictive contouring control for time-optimal quadrotor flight. IEEE Trans Robot 2022;38(6):3340–56.

[29] Shen X, Chen L, Lv Z, Wu Y. An adaptive controller for attitude tracking of a coaxial tilt-rotor UAV. In: 2022 37th youth academic annual conference of Chinese Association of Automation (YAC); IEEE; 2022. p. 410–15.
[30] Slotine J, Li WP. Applied nonlinear control. China Machine Press; 1991.
[31] Ta DA, Fantoni I, Lozano R. Modeling and control of a tilt tri-rotor airplane. In: 2012 American control conference (ACC); 2012. p. 131–36. https://doi.org/10.1109/ACC.2012.6315155
[32] Theys B, Dimitriadis G, Hendrick P, De Schutter J. Influence of propeller configuration on propulsion system efficiency of multi-rotor unmanned aerial vehicles. In: 2016 international conference on unmanned aircraft systems (ICUAS); IEEE; 2016. p. 195–201.
[33] Wang Q, Yang T, Liu G, Qin Y, Fang Y, Sun N. Adaptive compensation tracking control for parallel robots actuated by pneumatic artificial muscles with error constraints. IEEE Trans Ind Inf 2024;20(2):1585–95. https://doi.org/10.1109/TII.2023.3280321
[34] Witze A, Kowsky J. Nasa has launched the most ambitious mars rover ever built: here is what happens next. Nature 2020;584(7819):15–16.
[35] Xian B, Hao W. Nonlinear robust fault-tolerant control of the tilt trirotor UAV under rear servo's stuck fault: theory and experiments. IEEE Trans Ind Inf 2018;15(4):2158–66.
[36] Yang G, Zhu T, Yang F, Cui L, Wang H. Output feedback adaptive rise control for uncertain nonlinear systems. Asian J Control 2023;25(1):433–42.
[37] Yang T, Sun N, Liu Z, Fang Y. Concurrent learning-based adaptive control of underactuated robotic systems with guaranteed transient performance for both actuated and unactuated motions. IEEE Trans Neural Netw Learn Syst 2023;35(12):1–12. https://doi.org/10.1109/TNNLS.2023.3311927
[38] Yoo CS, Ryu SD, Park BJ, Kang YS, Jung SB. Actuator controller based on fuzzy sliding mode control of tilt rotor unmanned aerial vehicle. Int J Control Autom Syst 2014;12(6):1257–65.
[39] Yu L, He G, Zhao S, Wang X, Shen L. Immersion and invariance-based sliding mode attitude control of tilt tri-rotor UAV in helicopter mode. Int J Control Autom Syst 2021;19(2):722–35.
[40] Yu L, Zhang D, Zhang J. Transition flight modeling and control of a novel tilt trirotor UAV. In: 2017 IEEE international conference on information and automation (ICIA); 2017. p. 983–88. https://doi.org/10.1109/ICInfA.2017.8079045

## Author biography

**Mr. Longlong Chen** is currently working toward the Ph.D. degree with the School of Control Science and Engineering, Dalian University of Technology. His main research interests include intelligent control, nonlinear control, safety control, and the application of control theory in unmanned aerial vehicles.

**Dr. Yanmei Jia** received the Ph.D. degree in mathematics from the Dalian University of Technology, Dalian, China, in 2020. She joined the School of Science, Dalian Minzu University, Dalian, China, in 2021. Her current research interests include optimization and nonlinear control theory and control applications in unmanned aerial vehicles.

**Dr. Sihao Sun** is a postdoctoral researcher at Department of Cognitive Robotics (CoR), Delft University of Technology. He received A Ph.D. degree in aerospace engineering from Delft University of Technology, Delft, the Netherlands in 2020. From 2020 to 2023, was a postdoctoral researcher at the Robotics and Perception Group (RPG), University of Zurich, Switzerland, and then a postdoctoral researcher at the Robotics and Mechatronic Group (RaM), University of Twente, the Netherlands. He is the winner of the Best Paper Award of IEEE Robotics and Automation Letters (2021), and NWO (Dutch Research Council) Veni grant (2023). His research interests include system identification, aerial robotics, and nonlinear control.

**Dr. Zongyang Lv** (Corresponding author) received the M.S. degree in mechanical engineering and the Ph.D. degree in control theory and control engineering from the Dalian University of Technology, Dalian, China, in 2015 and 2021, respectively. From 2022 to 2023, he was a postdoctoral researcher with the Dalian University of Technology, Dalian, China. He is currently a postdoctoral researcher with the Department of Electrical and Computer Engineering, University of Alberta, Edmonton, Canada. He is the winner of the Best Paper Prize Award of IFAC Control Engineering Practice (2023). His research interests include nonlinear control, fixed-time control, and aerial vehicle control.

**Prof. Yuhu Wu** received the Ph.D. degree in mathematics from the Harbin Institute of Technology, Harbin, China, in 2012. Since 2012, he has held an Assistant Professor position with the Harbin University of Science and Technology, Harbin. He held a Postdoctoral Research position with Sophia University, Tokyo, Japan, from 2012 to 2015. In 2015, he joined the School of Control Science and Engineering, Dalian University of Technology, Dalian, China, where he is currently a Full Professor. His research interests relates to optimization, and nonlinear control theory and applications of control to Boolean networks, automotive powertrain systems, and unmanned aerial vehicles.